Chinese Chemical Letters 34 (2023) 108563

Contents lists available at ScienceDirect

Chinese Chemical Letters

journal homepage: www.elsevier.com/locate/cclet

In-situ construction of $Co(OH)_2$ nanoparticles decorated biochar for highly efficient degradation of tetracycline hydrochloride *via* peracetic acid activation

Fengbin Sun[a,b], Xudong Yang[c], Feng Shao[d], Fan Li[c], Zhicheng Pan[e], Lin Qiao[a,*], Ziniu Xiao[b,*], Wen Liu[c]

[a] *Institute of Urban Meteorology, China Meteorological Administration, Beijing 100089, China*
[b] *State Key Laboratory of Numerical Modeling for Atmospheric Sciences and Geophysical Fluid Dynamics, Institute of Atmospheric Physics, Chinese Academy of Sciences, Beijing 100029, China*
[c] *The Key Laboratory of Water and Sediment Sciences, Ministry of Education, College of Environmental Sciences and Engineering, Peking University, Beijing 100871, China*
[d] *College of Landscape Architecture, Zhejiang Agriculture and Forestry University, Hangzhou 311300, China*
[e] *Water Safety and Water Pollution Control Engineering Technology Research Center in Sichuan Province, Haitian Water Group, Chengdu 610299, China*

ARTICLE INFO

Article history:
Received 17 January 2023
Revised 11 April 2023
Accepted 9 May 2023
Available online 13 May 2023

Keywords:
Biochar
Peracetic acid (PAA)
Tetracycline hydrochloride
Intermediates
DFT calculation

ABSTRACT

Peracetic acid ($CH_3C(O)OOH$, PAA)-based heterogeneous advanced oxidation process (AOP) has attacked intensive interests due to production of various reactive species. Herein, $Co(OH)_2$ nanoparticles decorated biochar ($Co(OH)_2$/BC) was fabricated by a simple and controllable method, which was used to degrade tetracycline hydrochloride (TTCH) in water through PAA activation. The results indicated that 100% TTCH ($C_0 = 10$ μmol/L) degradation efficiency was realized within 7 min at pH 7, with a high kinetic rate constant (k_1) of 0.64 min^{-1} by the optimized $Co(OH)_2$/BC. Material characterizations suggested that $Co(OH)_2$ nanoparticle was successfully decorated on biochar, leading to more active sites and electronic structure alteration of biochar, thus greatly promoting the catalytic cleavage of PAA for radicals production. Then, the reactive oxygen species (ROS) quenching experiments and electron paramagnetic resonance (EPR) analysis demonstrated the key species were alkoxyl radicals (R–O$^{\bullet}$, mainly $CH_3CO_2^{\bullet}$ and $CH_3CO_3^{\bullet}$), HO$^{\bullet}$ and $^1O_2$ in this system. Besides, density functional theory (DFT) calculation on Fukui index further revealed that the vulnerable sites of TTCH and three possible degradation pathways were proposed. This study can provide a new strategy for synthesis functional materials in PAA activation AOPs for removal of antibiotics in water.

Water pollution problem caused by antibiotics has aroused serious threats to the ecosystem and human health in recent decades, as various antibiotics have been continuously detected in water/wastewater due to their wide application [1]. Tetracycline hydrochloride (TTCH), as a represent broad-spectrum antibiotic, is largely used to treat human diseases and livestock feeding [2]. Unfortunately, exceeded application of TTCH causes its transfer into water systems such as groundwater, surface water and even drinking water, leading to serious risks to ecosystem and human health [3,4]. However, the traditional wastewater treatment techniques fail to effectively remove antibiotics due to its complicated ring-structure and low-level concentration, thus developing novel treatment method is extremely necessary for TTCH contaminated water treatment.

Advanced oxidation processes (AOPs) are widely applied to remove organic pollutants owing to the advantages of strong radical production, easy operation and mild reaction conditions [5,6]. Peracetic acid ($CH_3C(O)OOH$, PAA), as a new oxidant, has attracted increasing attention in wastewater treatment area. PAA is the product of the reaction catalyzed by acetic acid (CH_3COOH, 3%-40%) and H_2O_2 (10%-40%). Due to its strong redox potential (1.06-1.96 V) [7], low toxic by-products production, high-cost effectiveness and environmental friendliness [8], catalytic PAA-based AOPs have been studied recently for organic pollutants degradation. PAA-based AOPs such as Co(II)/PAA and Fe(II)/PAA systems are constructed for pollutants degradation [8,9]. Previous studies have shown that Co(II) and Fe(II) ions as well as catalysts can effectively

* Corresponding authors.
E-mail addresses: bjs_qxt@sina.com (L. Qiao), xiaozn@lasg.iap.ac.cn (Z. Xiao).

https://doi.org/10.1016/j.cclet.2023.108563
1001-8417/

activate PAA to produce hydroxyl radical (•OH) and other alkoxyl radicals (R–O•) such as $CH_3CO_2^•$ and $CH_3CO_3^•$, since these transition metals can readily decompose peroxide bond (O–O) in PAA [9]. Meanwhile, the by-products of organic pollutants after degradation in PAA AOPs are less toxic comparing with traditional disinfectants application (*e.g.,* chlorine-based disinfectants), and the organic carbon provided by PAA is the key factor for decreased the toxicity [10]. Therefore, the PAA-based AOPs have a less adverse impact on ecosystem [11]. Thus, PAA is a good oxidant in AOPs for wastewater treatment, and efficient material is needed to highly activate PAA. Biochar (BC) belongs to an inexpensive and carbon-rich material, which can be produced from waste biomass in the absence of oxygen by thermochemical conversion [12–14]. Compared to other carbon materials (*e.g.,* activated carbon and carbon nanotubes), BC has various surface functional groups, porous structures, large surface area and low-cost, which has led to become a potential materials for pollutants removal [15]. The source of BC is rich in nature, such as crop residue, wood biomass and animal litter [12], leading to resource reuse, as well as high environmental and economic benefits. Moreover, it is reported to show ability to active persulfate (PS) in previous studies [16,17], which can promote the generation of reactive oxygen species (ROS). However, neat BC possesses a problem that it generally exhibits weak catalytic property for oxidant activation and slow kinetics for ROS production [18]. Although PAA can be activated by several pathways such as ultrasound, ultraviolet (UV) light, metal ions and catalysts [9], the Co(II)-based catalysts are demonstrated as an efficient way considering the high catalytic performance, low energy consumption, easy operation and high reusability [19,20]. To address the challenge on Co(II) leaching and possible adverse effect on environment, Co(II) active site can be anchored onto support such as BC to construct composite material. In addition, the BC support also can regulate the electronic structure of active Co(II) catalyst to improve its catalytic performance. Thus, a variety of composites have been developed including $Co(OH)_2$/g-C_3N_4 [21], $Co(OH)_2/WO_3$ [22] and $Co(OH)_2/KNbO_3$ [23] in heterogenous AOPs. However, few studies report preparation and application of $Co(OH)_2$ modified BC for PAA activation and pollutants degradation.

In this study, $Co(OH)_2$ nanoparticles decorated biochar ($Co(OH)_2$/BC) was prepared *via* a simple coprecipitation method and used to remove TTCH by activating PAA. Material characterizations have verified the successful modification of BC by $Co(OH)_2$ nanoparticles and its good catalytic performance. $Co(OH)_2$/BC displayed excellent degradation efficiency, as 100% of TTCH with an initial concentration of 10 μmol/L was degraded within 7 min at pH 7. Meanwhile, effect of pH and Co leaching also were evaluated. Furthermore, ROS scavenging experiments and electron paramagnetic resonance (EPR) were conducted to identify the primary reactive species contributed to TTCH degradation in this system. Finally, density functional theory (DFT) calculation on Fukui index illustrated the sites susceptible of TTCH to radical attack, and the possible degradation pathways were also proposed. This study can provide new insights into activation of PAA by cobalt-based materials and organics degradation.

All chemicals in this work are exhibited in Text S1 (Supporting information). The catalysts preparation process are also shown in Text S1.

Material characterizations were applied to determine the microstructure of as-prepared catalysts including scanning electron microscopy (SEM), transmission electron microscopy (TEM), high-resolution TEM (HRTEM), X-ray diffraction (XRD), X-ray photoelectron spectroscopy (XPS), Brunauer-Emmett-Teller (BET) specific surface area analysis and Fourier transform infrared spectrometer (FT-IR). The detailed characterization methods are documented in Text S2 (Supporting information). In addition, Text S3 (Supporting information) presents the detailed information on the methods of EPR analysis. The electrochemical properties of $Co(OH)_2$/BC and BC were also conducted on electrochemical workstation (CHI660, China), and the specific information is shown in Text S4 (Supporting information).

The TTCH degradation by PAA activation by using different materials were tested. The specific information can be observed in Text S5 (Supporting information). Besides, 10 mg material without PAA was added in the reaction system to investigate the adsorption of TTCH. The TTCH concentration was measured by a high-performance liquid chromatography (HPLC, Agilent 1260 Infinity II, USA), and the detailed methods including analysis of degradation intermediates/products are provided in Text S5. ROS quenching experiments were applied to examine their contribution to TTCH degradation. 100 mmol/L *tert*-butanol (TBA), ethanol (EtOH) and furfuryl alcohol (FFA) were applied to 1 mL to trap •OH, •OH and R-O•, and singlet oxygen ($^1O_2$), respectively [24]. Fukui function *via* DFT calculation was used to predict the regioselectivity of ROS to TTCH molecule using Gaussian 16 C.01 software and the specific information is described in Text S6 (Supporting information) [25,26].

Fig. 1a vividly shows the schematic on preparation process of $Co(OH)_2$/BC. After heating at 500 °C in N_2, BC would transfer into structure of highly ordered graphene [13]. After $Co(NO_3)_2{\cdot}6H_2O$ was evenly dispersed in solution and mixed with BC, $NH_3{\cdot}H_2O$ was added then as precipitator to *in-situ* generate $Co(OH)_2$ nanoparticles, which were decorated on BC for the formation of $Co(OH)_2$/BC. Figs. S1a-c (Supporting information) present the prepared neat BC exhibited sheet-like structure. Fig. S1d (Supporting information) of SEM image displays synthesized $Co(OH)_2$ exhibited as particles, and the lattice fringe distance was 0.459 nm (Fig. S1f in Supporting information), assigned to the (001) lattice plane of β-$Co(OH)_2$ (JCPDS card No. 30-0443) [22]. TEM and HRTEM images indicate that as-prepared $Co(OH)_2$/BC also presented as sheet-like structure (Figs. 1b–e), indicating the introduction of $Co(OH)_2$ had a slight effect on the basic structure of BC support. In addition, the HRTEM image shown in Figs. 1d and e indicate that the size of formed $Co(OH)_2$ nanoparticle was ∼10 nm, and it can be clearly seen that the $Co(OH)_2$ nanoparticles were successfully decorated on BC. Fig. 1e displays the lattice fringe distance of was $Co(OH)_2$ nanoparticle was 0.460 nm, corresponding to the (001) lattice plane of β-$Co(OH)_2$ (JCPDS card No. 30-0443) [22]. Figs. 1f and g also show $Co(OH)_2$/BC exhibited a sheet-like structure, consistent with the TEM results. Besides, the BET specific surface area and pore volume of prepared catalysts were also displayed in Figs. 1h and i and Fig. S2 (Supporting information). The neat BC showed a type IV isotherm with an obvious H4 hysteresis loop (Fig. 1h) [27], suggesting the emergence of mixed micropores and mesopores structure. The BET surface area of BC was 6.812 m^2/g, and the major pore size located at 2-4 nm (Fig. S3a in Supporting information). In comparison, $Co(OH)_2$/BC also exhibited type IV isotherms with H4 hysteresis loop, but its BET surface area was increased to 18.864 m^2/g due to $Co(OH)_2$ nanoparticles decoration. In addition, besides the primary pore size of 2-4 nm, another peak at ∼10 nm was also observed, which is attributed to the voids between BC and $Co(OH)_2$ nanoparticle. The enhanced BET surface benefits the interaction of active sites and PAA, thus promoting the catalytic reaction [28].

In the FT-IR spectra (Fig. 2a), BC displayed five peaks at 662, 867, 1436, 1589 and 3432 cm^{-1}, in which 662 and 867 cm^{-1} belonged to the bending vibration of –CH while 1436 cm^{-1} can be ascribed as the bending vibration of $–CH_2$ [18,29]. Meanwhile, the 1589 cm^{-1} peak was attributed to the stretching vibration of C=C, and 3432 cm^{-1} to the stretching vibration of –OH [30]. For $Co(OH)_2$/BC after introduction of $Co(OH)_2$ (Fig. 2a), all peaks slightly shifted to low wavenumber, indicating that the chemical bond of materials was altered. In comparison, in the FT-IR spectra of neat $Co(OH)_2$ (Fig. 2a), the emergence of Co–O and Co–OH

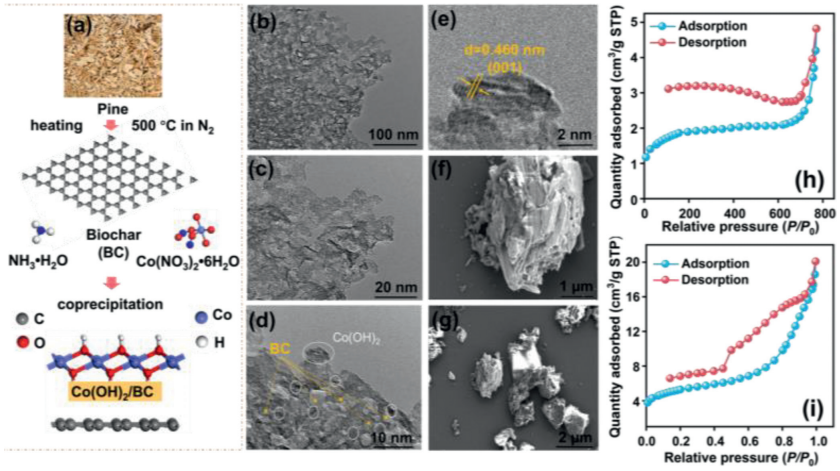

Fig. 1. (a) The preparation process of $Co(OH)_2$/BC. (b-e) TEM and HRTEM images of $Co(OH)_2$/BC. (f, g) SEM images of $Co(OH)_2$/BC. N_2 adsorption-desorption curves of (h) pure BC and (i) $Co(OH)_2$/BC.

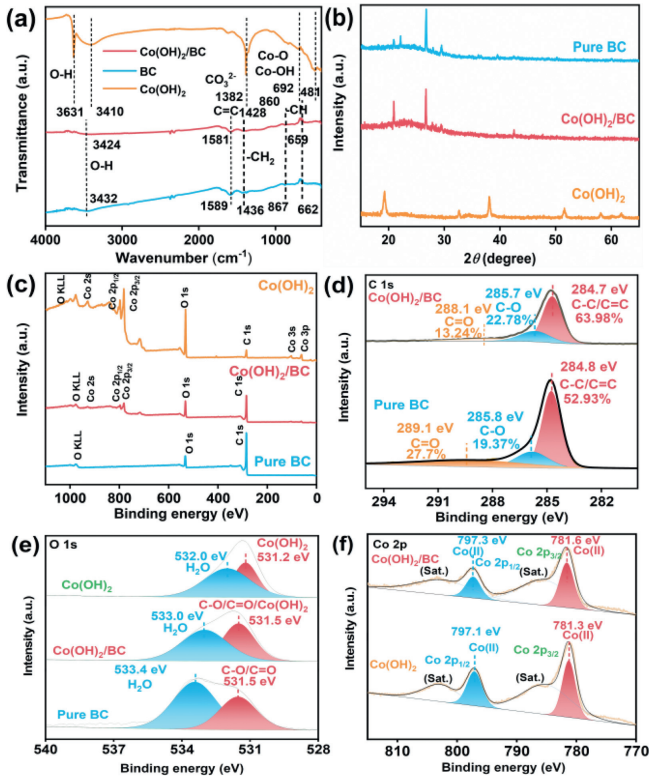

Fig. 2. (a) FT-IR spectra and (b) XRD patterns of materials. (c) XPS survey spectra, high-resolution XPS spectra of (d) C 1s, (e) O 1s and (f) Co 2p.

at 481 and 692 cm^{-1} have verified the successful preparation of $Co(OH)_2$ [30]. However, it can hardly find the characteristic peaks of $Co(OH)_2$ in $Co(OH)_2$/BC, owing to the low content of $Co(OH)_2$ in the composite material. In the XRD patterns (Fig. 2b), the peaks of neat $Co(OH)_2$ at 19.29°, 32.56° and 38.09° can be classified as the β-$Co(OH)_2$ (JCPDS card No. 30-0443) [22], corresponding to (001), (100) and (101) lattice plane, respectively. For neat BC, there was a sharp peak at 26.72°, assigned to the characteristic peak of pine biochar [13]. For $Co(OH)_2$/BC, the two apparent peaks at 20.94° and 26.76°, the peak at 20.94° was the (001) lattice plane of $Co(OH)_2$, indicating its successful decoration. Meanwhile, the slight alteration of BC characteristic peaks (from 26.72° to 26.76°) also indicated the successful introduction of $Co(OH)_2$. The XPS survey spectra in Fig. 2c obviously shows that $Co(OH)_2$/BC contained elements of Co, O and C. Then, the high-resolution XPS spectra of C 1s in Fig. 2d shows the neat BC had three main peaks at 284.8, 285.8 and 289.1 eV, indexed to the C–C/C=C, C–O and C=O, respectively [18]. However, all the peaks shifted to the low binding energy for $Co(OH)_2$/BC in Fig. 2d, suggesting the surface electronic density decreased for $Co(OH)_2$ and electronic transfer direction occurred from $Co(OH)_2$ to BC [19]. In addition, the high-resolution XPS spectra of O 1s (Fig. 2e) displays BC owned two peaks at 531.5 and 533.4 eV, assigned to the C–O/C=O and adsorbed O (OA, from adsorbed H_2O/OH group), respectively [19]. For $Co(OH)_2$, there were two apparent peaks at 531.2 and 532.0 eV, which can be classified as the lattice O (O_L) and O_A, respectively [18]. For $Co(OH)_2$/BC, the two peaks shifted to 531.5 and 533.0 eV compared with neat BC and $Co(OH)_2$ (Fig. 2e), confirming the formation of composites. In addition, in the Co 2p of neat $Co(OH)_2$ spectra (Fig. 2f), the two apparent peaks at 781.3 and 797.1 eV can be ascribed to Co $2p_{3/2}$ and Co $2p_{1/2}$ of Co(II), respectively [19]. Compared with neat $Co(OH)_2$, the binding energy of the two peaks in $Co(OH)_2$/BC changed to 781.6 and 797.3 eV with a positive alternation (Fig. 2f), suggesting that $Co(OH)_2$ electron transfer would occur from $Co(OH)_2$ to BC in the composite, thus facilitating catalytic activation of PAA.

To further confirm the high electron transfer ability of $Co(OH)_2$/BC, a series of photoelectric characterizations were performed (Fig. S3 in Supporting information). The electrochemical impedance spectroscopy (EIS) revealed $Co(OH)_2$/BC had smaller arc radius than BC, indicating its lower resistance of electronic transfer and improved charge transfer efficiency [31]. In addition, the spectra of cyclic voltammetry (CV) and linear sweep voltammetry (LSV) also present $Co(OH)_2$/BC exhibited a higher current density and redox capacity than BC, indicating the electrical conductivity and catalytic activity of $Co(OH)_2$/BC was greatly enhanced [31].

Fig. 3a presents the degradation of TTCH in different PAA activation systems and the relevant first-order rate constants (k_1, $\ln(C_0/C_t) = k_1 t$) are displayed in Fig. S4a (Supporting information). PAA only could hardly degrade TTCH, and $Co(OH)_2$/BC only also could not remove TTCH through adsorption. However, $Co(OH)_2$/BC composites could efficiently activate PAA for TTCH degradation. The removal efficiency of TTCH after PAA activation by $Co(OH)_2$/BC composites with different Co contents all reached >95%, Specifically, the TTCH removal efficiency was 96.5% for 1 wt% $Co(OH)_2$/BC in 10 min, 100% for 5 wt% $Co(OH)_2$/BC in 10 min, 100% for 10 wt% and 20 wt% $Co(OH)_2$/BC in 7 min, respectively. In addition, the k_1 was gradually increased from 0.30 to 0.90 min^{-1} (Fig. S4a). Thus, 10 wt% $Co(OH)_2$/BC was selected as the optimized catalyst for fur-

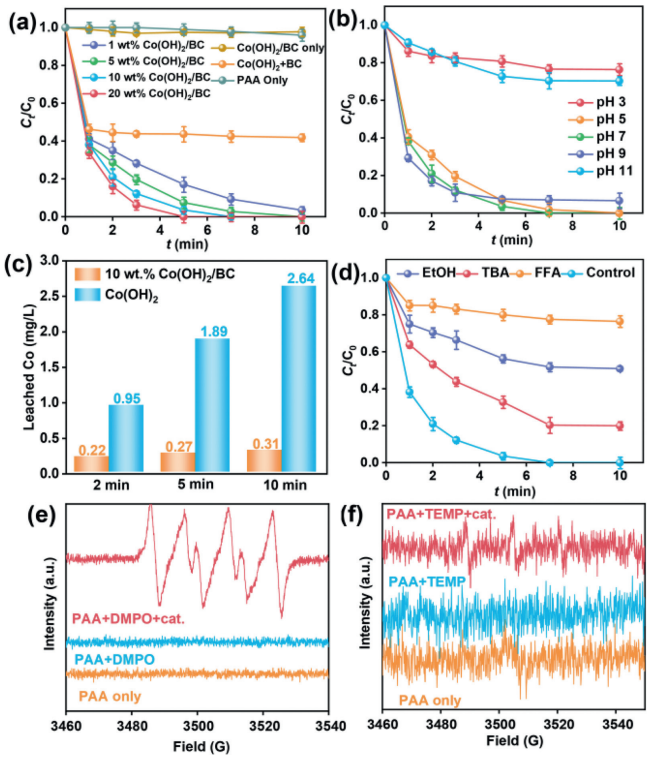

Fig. 3. (a) Degradation of TTCH by various materials. (b) Effect of pH on TTCH degradation after PAA activation by 10 wt% $Co(OH)_2$/BC. (c) Measurement on leached Co content of 10 wt% $Co(OH)_2$/BC and neat $Co(OH)_2$ during reaction. (d) TTCH degradation kinetics in the presence of different scavengers. (e) EPR spectra of DMPO-$^{\bullet}$OR and $^{\bullet}$OH. (f) EPR spectra of TEMP-$^1O_2$. Experimental conditions: initial TTCH = 10 μmol/L, pH = 7.0 ± 0.2 except for (b), PAA concentration = 100 μmol/L, material dosage = 0.1 g/L.

ther studies considering its both high catalytic property and low Co content.

In addition, neat BC showed relatively low catalytic activity on PAA activation and TTCH removal due to the low k_1 value of 0.01 min^{-1} (Figs. S4a and b in Supporting information). Thus, although BC alone failed to effectively active PAA and remove pollutants, it can play a crucial role in regulating the electronic structure of $Co(OH)_2$, which has promoted the ability of $Co(OH)_2$ for PAA activation and TTCH degradation based on the results of XPS and degradation experiments. The neat $Co(OH)_2$ also showed a lower k_1 value (0.18 min^{-1}) than 10 wt% $Co(OH)_2$/BC (0.64 min^{-1}) for TTCH degradation (Fig. S5 in Supporting information). In comparison, a mixture of $Co(OH)_2$ and BC was used for PAA activation and TTCH degradation, it is found that only 58.1% TTCH was removed with a low k_1 of 0.05 min^{-1}, implying the chemical bonding of $Co(OH)_2$ nanoparticle and BC in the composite $Co(OH)_2$/BC, rather than simply mixing.

Fig. 3b presents that the impact of pH on TTCH degradation by 10 wt% $Co(OH)_2$/BC, and the relevant k_1 values are shown in Fig. S4c. Fig. 3b indicates complete degradation of TTCH was realized at pH 5 and 7, with k_1 of 0.54 and 0.64 min^{-1}, respectively. TTCH also showed high degradation efficiency at pH 9 (93.4%), with k_1 of 0.23 min^{-1}. However, at pH at 3 or 11, the degradation efficiency was dramatically inhibited to 23.7% and 29.7%, with a low k_1 of 0.022 and 0.035 min^{-1}, respectively. pH is highly related to the existing forms of PAA and TTCH (Fig. S4d in Supporting information). At pH 3, the main form of TTCH was $TTCH^+$, so the material could hardly adsorb $TTCH^+$, as the zero-point charge (pHPZC) of $Co(OH)_2$/BC was 4.56 as shown in Fig. S6 (Supporting information), leading to low efficiency of removal TTCH at pH 3 [32]. In addition, PAA ($pK_a = 8.2$) existed as PAA anion (PAA^-) at pH 11 according to the previous study for the speciation and decomposition of PAA [8], which was a scavenger for generated ROS. Relatively low content was leached during reaction (only 0.31 mg/L at 10 min) as shown in Fig. 3c, suggesting the developed material had good stability. In comparison, after PAA activation at 10 min, the neat $Co(OH)_2$ showed an extremely high Co leaching concentration of 2.64 mg/L, so anchoring of $Co(OH)_2$ nanoparticle on BC exactly promote the stability of material. In addition, naproxen (NAP), diclofenac (DCF), gatifloxacin (GAT) and acetylaminophenol (ACE) also were applied to verify the universality of the system. The result shows that the removal rates of NAP, DCF, GAT and ACE at 10 min were achieved as 91.6%, 98.1%, 92.8% and 92.9%, respectively (Fig. S7 in Supporting information). Given the material adsorption only contributed <5% removal for all four contaminants, degradation still played the dominant role, further indicating the as-prepared materials possesses excellent universality for PAA heterogeneous catalytic activation system. Finally, other related catalysts used in PAA activation for pollutants removal were also compared with $Co(OH)_2$/BC in Table S4 (Supporting information). The result indicates that the prepared materials possess excellent ability to remove pollutants *via* PAA activation [33].

The scavenger quenching experiments were further carried out to verify ROS contributions to TTCH degradation (Fig. 3d). After adding TBA, the removal efficiency decreased from 100% to 80.1%, indicating $^{\bullet}$OH played a less important role. After the addition of EtOH, the TTCH degradation efficiency decreased to the 49.1%, indicating alkoxyl radicals ($^{\bullet}$O–R, mainly $CH_3CO_2^{\bullet}$ and $CH_3CO_3^{\bullet}$) played important roles in TTCH degradation [9]. Then, the addition of FFA also greatly inhibited the TTCH degradation efficiency by 23.6%, suggesting that $^1O_2$ also played a vital role; and moreover, $^1O_2$ may be related to the formation of other radicals such as alkoxyl radicals [34]. In addition, previous study revealed that TBA and FFA may have some effects on PMS/PDS activation system [35]. Given PAA activation system may also share $^{\bullet}$OH and $^1O_2$, it will be interesting to study whether TBA and FFA would induce unique effects on reactive species generation in PAA in future. The result of ROS quenching tests illustrated that $^{\bullet}$O–R, $^{\bullet}$OH and $^1O_2$ all played irreplaceable roles in the degradation of TTCH on the whole. In addition, EPR technology was applied to identify the generated ROS. Fig. 3e presents $CH_3CO_3^{\bullet}$ ($\alpha_H = 11.7$ G, $\alpha_N = 14.3$ G, $\alpha_{H\gamma} = 1.4$ G) and $^{\bullet}$OH ($\alpha_H = 14.9$ G, $\alpha_N = 14.9$ G) were detected using DMPO as the trapping agent in methanol and water, respectively [36]. However, $CH_3CO_2^{\bullet}$ was hard to identify, because it could easily react with PAA to generate $CH_3CO_3^{\bullet}$ and decomposed through self-decay or self-coupling [11]. Furthermore, Fig. 3f shows three characteristic peaks of TEMP-$^1O_2$ in the PAA activation system, which displayed an intensity of 1:1:1 and $\alpha = 17.2$ G. Accordingly, EPR also demonstrated that the formation of $^{\bullet}$OH, $^{\bullet}$O–R and $^1O_2$ in PAA activation system, which is in good agreement with the ROS quenching results.

DFT calculation was utilized to predict the reactive sites of TTCH in theory. Fig. 4a displays the geometry model of TTCH molecule. Figs. 4b and c present the relevant highest occupied molecular orbital (HOMO) and the lowest occupied molecular orbital (LOMO). It can be observed that the HOMO is mainly located around the N9 atom of TTCH, indicating this site can be easily attacked by ROS for oxidation reaction. In the ESP spectra (Fig. 4d), the yellow regions represent the sites can obtain electrons and purple regions represent the sites will lose electrons during the reaction.

Thus, N9 and N10 regions are likely to be attacked by ROS, which is consistent with the HOMO distribution. In general, the generated ROS ($^{\bullet}$OH, $^{\bullet}$O–R and $^1O_2$) in this system can be classified by electrophilic species [37], thus the Fukui function index (f^-) towards electrophilic attack is calculated and shown in Fig. 4e to

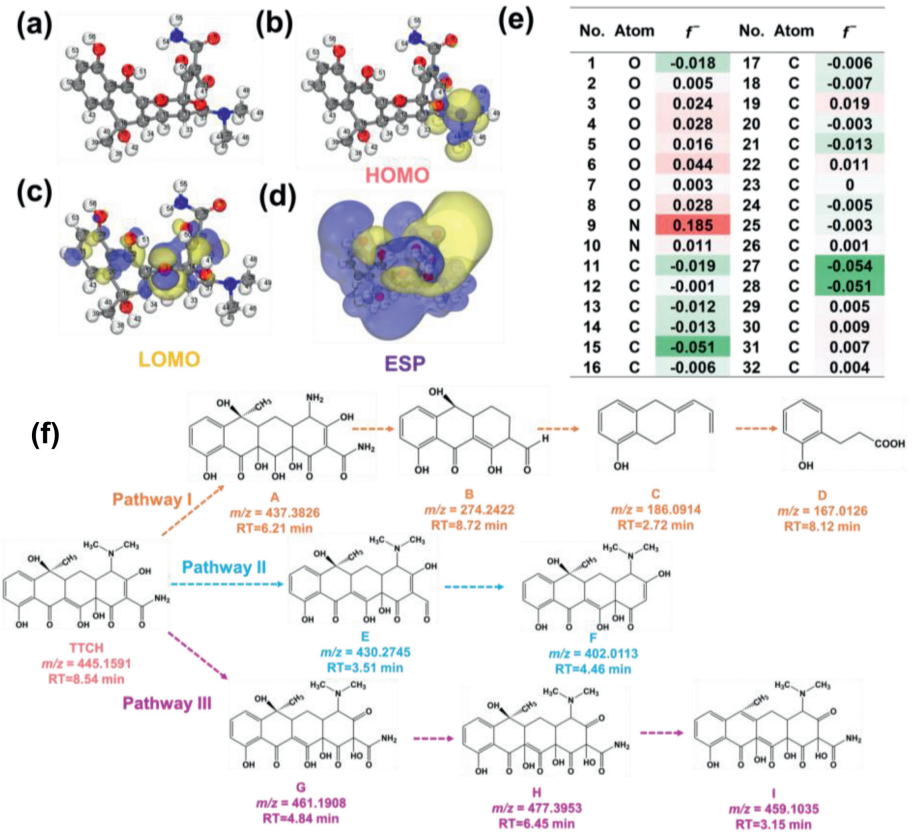

No.	Atom	f^-	No.	Atom	f^-
1	O	-0.018	17	C	-0.006
2	O	0.005	18	C	-0.007
3	O	0.024	19	C	0.019
4	O	0.028	20	C	-0.003
5	O	0.016	21	C	-0.013
6	O	0.044	22	C	0.011
7	O	0.003	23	C	0
8	O	0.028	24	C	-0.005
9	N	0.185	25	C	-0.003
10	N	0.011	26	C	0.001
11	C	-0.019	27	C	-0.054
12	C	-0.001	28	C	-0.051
13	C	-0.012	29	C	0.005
14	C	-0.013	30	C	0.009
15	C	-0.051	31	C	0.007
16	C	-0.006	32	C	0.004

Fig. 4. (a) The geometry of TTCH molecule. (b) HOMO and (c) LOMO of TTCH. (d) ESP mapping of TTCH. (e) Fukui index of TTCH. (f) Proposed degradation pathway of TTCH in $Co(OH)_2$/BC activated PAA system.

investigate the reactive sties of TTCH. It is indicated that the reactive sites of N9 ($f^- = 0.185$), N10 ($f^- = 0.011$), C19 ($f^- = 0.019$) and C22 ($f^- = 0.011$) with high Fukui index prefer to be attacked by ROS. Subsequently, the possible degradation pathway of TTCH is also proposed based on degradation intermediates determination. The transformation products (TPs) of TTCH were measured using a Q ExactiveTM Plus Quadrupole OrbitrapTM mass spectrometer system (Thermo Fisher Scientific, USA) system with an electrospray ionization (ESI) source (Thermo Scientific, USA). Three possible degradation pathways were proposed in Fig. 4f and detailed information of TPs was listed in Table S5 (Supporting information). For pathway I, the N9 ($f^- = 0.185$) underwent attack for demethylation, product **A** ($m/z = 437.3826$) was formed [38]. Then, further attack of **A** by ROS led to ring-open reactions for the formation of product **B** ($m/z = 274.2422$), **C** ($m/z = 186.0914$) and **D** ($m/z = 167.0126$) [39]. For pathway II, N10 ($f^- = 0.011$) was attack *via* a deamination way, and product **E** ($m/z = 430.2745$) was formed [40]. Then, product **E** was further transferred to product **F** ($m/z = 402.0113$) and finally formed inorganic substances. For Pathway III, a hydroxyl addition reaction occurred at the C22 ($f^- = 0.011$) site, leading to the formation of product **G** ($m/z = 461.1908$) [40]. Product **G** was further become **H** ($m/z = 477.3953$) through hydroxylation and **I** ($m/z = 459.1035$) through demethylation [40]. Finally, deep oxidation products such as small molecular acids, CO_2 and H_2O could be formed. Consequently, the degradation pathway is well consistent with the DFT calculation.

In conclusion, $Co(OH)_2$/BC composite was prepared by a simple and controllable method, which achieved efficient removal of TTCH after PAA activation. The optimized 10 wt% $Co(OH)_2$/BC could completely degrade TTCH after PAA activation within 7 at pH 7 min, with a high reaction rate constant (k_1) of 0.64 min^{-1}. The introduction of BC caused alteration of electronic structure of $Co(OH)_2$, leading to higher electron transfer efficiency for PAA activation. ROS quenching experiments and EPR analysis indicated that ROS including alkoxyl radicals (R–O•, mainly CH_3CO_2• and CH_3CO_3•), HO• and $^1O_2$ played important roles in TTCH degradation in this system. DFT calculation has revealed the atoms of TTCH with high Fukui index (f^-) are the active sites for ROS electrophilic attack. The degradation pathway of TTCH in this system primarily includes demethylation, deamination and hydroxylation. The developed $Co(OH)_2$/BC in this work exhibit good application potential in degradation of emerging pollutants in water.

Declaration of competing interest

The authors declare that they have no known competing financial interests or personal relationships that could have appeared to influence the work reported in this paper.

Acknowledgments

This work is supported by the National Key Research and Development Program of China (Nos. 2022YFF1303102 and 2021YFA1202500), Beijing Natural Science Foundation (No. 8232035), the National Natural Science Foundation of China (Nos. 52270053, 52200083 and 52200084), the Beijing Nova Program (No. 20220484215), and the Key Special Projects for Science and Technology of Inner Mongolia (No. 2021EEDSCXSFQZD001).

Supplementary materials

Supplementary material associated with this article can be found, in the online version, at doi:10.1016/j.cclet.2023.108563.

References

[1] W. Wang, X. Li, F. Deng, et al., Chin. Chem. Lett. 33 (2022) 5200–5207.
[2] A. Wang, Z. Zheng, H. Wang, et al., Appl. Catal. B 277 (2020) 119171.
[3] J. Yu, J. Kiwi, I. Zivkovic, et al., Appl. Catal. B 248 (2019) 450–458.
[4] B. Zhang, X. He, C. Yu, et al., Chin. Chem. Lett. 33 (2022) 1337–1342.
[5] P. Dumrongrojthanath, T. Thongtem, A. Phuruangrat, S. Thongtem, Superlattices Microstruct 64 (2013) 196–203.
[6] K. Tian, L. Hu, L. Li, et al., Chin. Chem. Lett. 33 (2022) 4461–4477.
[7] X. Chen, J. Wang, Chem. Eng. J. 395 (2020) 125095.
[8] J. Kim, T. Zhang, W. Liu, et al., Environ. Sci. Technol. 53 (2019) 13312–13322.
[9] Z. Wang, J. Wang, B. Xiong, et al., Environ. Sci. Technol. 54 (2019) 464–475.
[10] S.R. Yang, C.S. He, Z.H. Xie, et al., Water Res. 217 (2022) 118402.
[11] P. Du, J. Wang, G. Sun, L. Chen, W. Liu, Water Res. 212 (2022) 118113.
[12] M. Ahmad, Y.S. Ok, A.U. Rajapaksha, et al., J. Hazard. Mater. 301 (2016) 179–186.
[13] T. Wang, S. Liu, W. Mao, et al., J. Hazard. Mater. 389 (2020) 121827.
[14] X. Xiong, Z. Liu, L. Zhao, et al., Chin. Chem. Lett. 33 (2022) 3097–3100.
[15] Y. He, X. Zhao, S. Zhu, et al., Sci. Total Environ. 871 (2023) 162046.
[16] C. Yu, X. Zhu, A. Mohamed, et al., J. Hazard. Mater. 442 (2023) 129927.
[17] R. Guo, B. Xi, C. Guo, et al., Environ. Funct. Mater. 1 (2022) 67–91.
[18] M. Xiong, J. Yan, G. Fan, et al., Chem. Eng. J. 444 (2022) 136589.
[19] W. Zhang, J. Liu, J. Tan, H. Yu, X. Liu, J. Clean. Prod. 340 (2022) 130714.
[20] J. Qi, J. Liu, F. Sun, et al., Chin. Chem. Lett. 32 (2021) 1814–1818.
[21] S. Mao, P. Zhao, Y. Wu, et al., Chem. Eng. J. 451 (2023) 138503.
[22] X. Tao, P. Pan, T. Huang, et al., Chem. Eng. J. 395 (2020) 125186.
[23] J. Qi, X. Yang, P.Y. Pan, et al., Environ. Sci. Technol. 56 (2022) 5200–5212.
[24] L. Kong, G. Fang, Z. Fang, et al., Chem. Eng. J. 416 (2021) 128996.
[25] W. Liu, Y. Li, F. Liu, et al., Water Res. 151 (2019) 8–19.
[26] H. Zhang, C. Xie, L. Chen, et al., Water Res. 229 (2022) 119392.
[27] A.T. Krzyżak, I. Habina-Skrzyniarz, G. Machowski, W. Mazur, Superlattices Microstruct 298 (2020) 110003.
[28] D. Huang, X. Sun, Y. Liu, et al., Chin. Chem. Lett. 32 (2021) 2787–2791.
[29] S. Zhu, X. Huang, F. Ma, et al., Environ. Sci. Technol. 52 (2018) 8649–8658.
[30] Y. Yang, P. Zhu, L. Zhang, et al., ACS Sustain. Chem. Eng. 7 (2019) 16803–16813.
[31] X. Yang, F. Li, W. Liu, et al., Appl. Catal. B 324 (2023) 122202.
[32] W. Zhang, Y. Peng, Y. Yang, Chem. Eng. J. 430 (2022) 132963.
[33] M.F. He, W.Q. Li, Z.H. Xie, et al., Water Res. 222 (2022) 118887.
[34] X. Yang, J. Duan, J. Qi, et al., J. Hazard. Mater. 445 (2023) 130576.
[35] Z.H. Xie, C.S. He, H.Y. Zhou, et al., Environ. Sci. Technol. 56 (2022) 8784–8795.
[36] L. Chen, J. Duan, P. Du, et al., Water Res. 221 (2022) 118747.
[37] J. Duan, L. Chen, H. Ji, et al., Chin. Chem. Lett. 33 (2022) 3172–3176.
[38] H. Liu, J. Qu, T. Zhang, et al., Environ. Pollut. 258 (2020) 113702.
[39] J. Guo, A. Zhang, Z. Pei, Sep. Purif. Technol. 287 (2022) 120568.
[40] C. Liu, H. Dai, C. Tan, et al., Appl. Catal. B 310 (2022) 121326.